AIAA JOURNAL
Vol. 46, No. 1, January 2008

Vortex Formation Process of a Starting Square Jet

S. C. M. Yu,* J. J. Ai,† L. Gao,‡ and A. W. K. Law§
Nanyang Technological University, Singapore 639798, Republic of Singapore

DOI: 10.2514/1.29514

This paper presents results of an experimental study on starting square jets at Reynolds numbers ranged from 2000 to 5000 (based on the jet diameter and the bulk mean velocity on the jet exit plane) using planar laser induced fluorescence for flow visualization and particle image velocimetry for velocity measurements, respectively. Similar to starting a circular jet at Reynolds numbers below 3000, vortex leapfrogging was found to appear, whereas pinch-off for the leading vortex ring was observed at higher Reynolds numbers. The "imperfect" leapfrogging between the third and the fourth vortex rings promoted growth of instability, which had led to the transition to turbulence for the entire jet. The maximum circulation that a vortex ring can attain during its formation is reached at the nondimensional time ($t^* = tW_0/D_e$) within the range of 1.6 to 2.4. The pinch-off of the leading vortex ring appeared shortly after the jet initiation for Reynolds numbers above 3000. Axis switching was found to play an important role for the vortex development in starting square jets. The interaction between the axis-switched vortex ring and the square-shaped jet stem facilitated the generation of contrarotating streamwise vortices at the corners of the jet stem. They were actually rotating in the opposite sense as those responsible for axis switching, and their existence had facilitated the thinning of the jet stem, causing a fast pinch-off for the leading vortex ring.

I. Introduction

THE present investigation concerns the impulsively started jet flow discharging from a square nozzle. In recent decades, the topic of noncircular jets has attracted a large number of researchers because of its priority in mixing enhancement. The velocity characteristics in both subsonic and supersonic regimes have been examined in detail; see, for example, Quinn and Militzer [1,2], Grinstein et al. [3,4], and Wang et al. [5]. It is well established that the corners of the square nozzle will facilitate the formation of contrarotating vortices, which might, in turn, lead to the axis-switching phenomenon [6,7]. Mixing and entrainment would be enhanced as a result, when compared with those of a circular jet under the same flow conditions [4]. In the square jets with periodical forcing, Grinstein and DeVore [4] found dependence of the occurrence of axis switching on the initial conditions, including the ratio of nozzle diameter to the momentum thickness, initial turbulence level, azimuthal momentum thickness distribution, and Reynolds number, by examining the time average jet properties. The important role of braid vortices in axis switching had also been recognized. Recently, the study on the process of evolution of the streamwise vortices for steady sudden-expansion square flows by Sau [8] revealed a type of wall vortices induced by the initial streamwise vortices. The fast growth of these wall vortices facilitates the quick outward spreading of the jet along the two principle planes of symmetry. The dynamic of the streamwise vortices in the starting square jet is therefore of great interest in present investigation.

For starting circular jets, notable works such as Gharib et al. [9] and Mosheni and Gharib [10], have investigated the phenomenon of vortex ring formation in a piston/cylinder arrangement. They have demonstrated that for a nonimpulsively started jet, a universal time scale for vortex ring formation could be obtained. This time scale, known as the formation number (L/D or $U_p t/D$), is the time when the vortex ring reaches its maximum circulation and energy, which also physically coincides with the pinch-off of the vortex ring in terms of its entrainment, velocity, and vorticity fields from its generating axisymmetric jet. A value of four for the formation number was identified from the experiments. Our earlier flow visualization investigation on a gravity-driven starting square jet (Ai et al. [11]) revealed that for Reynolds numbers below 5000, the normalized value for the pinch-off time was estimated to be at about seven and was similar to that found in a circular jet under the same setup. Moreover, the pinch-off conditions depended on many factors (Linden and Turner. [12]). A nonuniform exit velocity profile may increase or decrease the formation number considerably. The time history of the piston movement and the boundary-layer characteristics at the jet exit are important factors as well. The roll up of additional vortices in the trailing jet, a result of Kelvin–Helmholtz instability, may also affect the formation number; see, for example, the computational studies by Zhao et al. [13].

The flow visualization results of Ai et al. [11] also showed that the jet tip was found to travel slower in square jets compared with a circular jet, and its penetration rate was almost constant within the first four diameters from the exit plane. It reached an asymptotic behavior thereafter (which was inversely proportional to the square root of time). The expansion rate of the head vortex core was proportional to time [2].

In the present investigation, extensive visualization tests using the planar laser induced fluorescence (PLIF) method and velocity measurements obtained by particle image velocimetry (PIV) on successive cross-sectional planes has shown further that axis switching is indeed closely related to the pinch-off process. The pinch-off for the leading vortex for the square jet is actually faster than the circular jet at the same Reynolds number. Some new flow structures have been identified, and they may be unique to the starting square jet phenomenon. The mechanism for the variation in the formation of streamwise vortices was also examined and compared with existing results on a steady square jet.

Reynolds numbers ranging from 2000 to 5000 were chosen to be examined in detail. The gravity-driven arrangement may provide an impulsive start for the jet under consideration. This range of Reynolds numbers was chosen after extensive flow visualization experiments that showed that transition to turbulence did not appear rapidly after the jet was initiated. The experimental arrangement will first be addressed. The results are presented and discussed in Sec. III. Because of space constraints, only the most representative results are to be shown here. Further details can be found in Ai [14]. The paper ends with brief concluding remarks.

Received 28 December 2006; accepted for publication 17 September 2007.

*Associate Professor, School of Mechanical and Aerospace Engineering.
†Research Scientist; currently, ShouGang Research Institute of Technology, 100041 Beijing, People's Republic of China.
‡Graduate Student, School of Mechanical and Aerospace Engineering.
§Research Scientist, School of Civil and Environmental Engineering.

II. Experimental Setup

The experimental rig and the coordinate system adopted are shown in Fig. 1a. The same rig had been used for both PLIF and PIV experiments. The test section was made of transparent Plexiglas to ensure optical access. Water was delivered to the test tank through the inlet, and a constant water level was maintained during the experiments. Fine wire mesh and honeycomb were installed between the tank and the converging duct to reduce the turbulence level of the inlet flow. The water driven by gravity was accelerated through the converging nozzle before discharging into the test tank with a cross-sectional area of 400×400 mm and 1000 mm in length. The initial turbulence intensity measured at the nozzle exit was about $0.5 \sim 0.6\%$ using a laser Doppler anemometer. The flow rate was monitored by a flowmeter (Endress & Hauser model Promag 33) and adjusted by a control valve that was fixed at the end of the rig. For measurements on respective cross-sectional planes, a mirror was positioned at far downstream and was tilted at 45 deg to the flow direction. The solenoid valve had an opening time of about 20 ms, ensuring that the opening sequence was almost immediate.

A. Nozzle Configurations

The nozzle contour was designed to follow a family of high-order polynomial shapes, as shown in Fig. 1b. The equivalent diameter of the square nozzle D_e can be calculated by the following equation:

$$\frac{\pi}{4}D_0^2 = \frac{\pi}{4}D_e^2 = a^2 \Rightarrow D_0 = D_e = \frac{2}{\sqrt{\pi}}a \tag{1}$$

where a is the width of the square nozzle, and D_0 is the exit diameter of the circular nozzle. So the inner width of the nozzle was 32 mm with an equivalent diameter $D_e = 36$ mm. Therefore, the Reynolds number can be defined as

$$Re = \frac{W_0 D_e}{\nu} \tag{2}$$

where ν is the kinematic viscosity.

B. Flow Visualization Experiment

The PLIF technique had been used to examine the vortex evolution of the square starting jets. For aqueous-phase experiments, the choice of tracer is determined by the following considerations [15]: The dye must be water soluble and stable under the laser excitation power needed to provide signal levels adequate for mixing measurements. It must also have absorption and emission spectra separated enough to avoid absorption of the emitted fluorescence wavelengths within the flow facility (optical trapping). 2,7–dichlorofluorescein (C20H10Cl2O5, $MW = 401.21$) was chosen as the dye tracer in our experiments. The dye was first dissolved in a small quantity of ethanol, which was subsequently diluted in water.

C. Experimental Procedures Using PLIF

As mentioned in the preceding section, the fluorescent dye prepared in a solution of alcohol has the property of fluorescing green when illuminated by laser light. Illumination was provided by a light sheet (about 3 mm thick) produced by passing the beam from a 5W argon-ion laser (SpectraPhysics) through a cylindrical lens. The pictures were recorded by digital camera (Kodak) with 12 bits and high resolution (1×1 K). The shutter speed was set at $1/125$ s, which was quick enough to capture the instantaneous features of the jet as it evolved in time. The frame rate was at 12.5 frames per second. The surrounding fluid containing no dye would appear black in the background of the captured images. A series of flow visualization experiments were conducted with Reynolds numbers ranged from 2000 to 5000. Three Reynolds numbers were chosen from the series for PIV measurements. Table 1 shows the experimental conditions for these three cases.

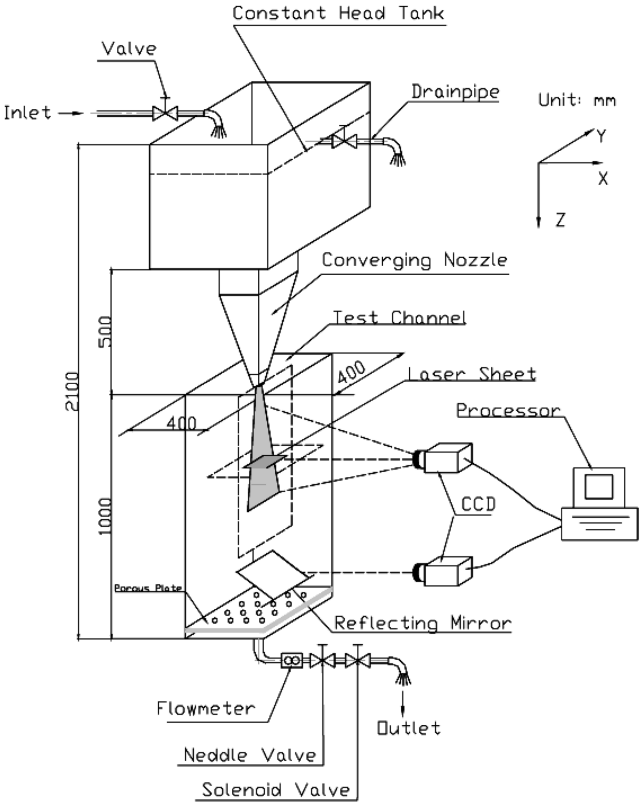

a) Schematic diagram of the experimental rig

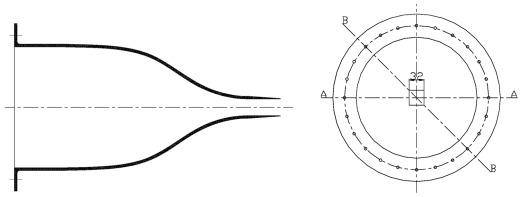

b) Nozzle geometry

Fig. 1 Experimental arrangements.

D. Particle Image Velocimetry

The PIV light source employed a dual-cavity-pulsed mini Nd: YAG laser with a maximum repetition rate of 15 Hz for each cavity. The energy level was 50 mJ per pulse and the pulse duration was about 7 ns. The emitted laser light was green with a wavelength of 532 nm. The light sheet had a typical thickness of 3 mm and a typical divergence angle of 32 deg. The double-image 8-bit digital CCD camera (Kodak Megaplus ES1.0) was configured. The spatial resolution of the cameras was 1008×1016 pixels. The camera was fitted with Nikon 60-mm lens. The interrogation area was set as an approximate size of 30×30 cm. The near neutral buoyant polymid particles with mean diameter of 50 μm were chosen as the seeding particles (density $= 1.03$ g/cm^3, size distribution $30 \sim 70$ μm, refractive index $= 1.5$). When conducting the experiments, the image capturing frequency was set to 6.25 Hz, which was half of that used in the PLIF experiments. The time interval between the two consecutive images varies with the initial condition to satisfy the criteria for cross correlation. The error in the velocity magnitude was estimated to be less than 2%. Further details can be found in Ai [14].

The vorticity ω was calculated by the vector field measured on the X–Z plane (c.f. Fig. 1a) as

$$\omega = \frac{\partial U}{\partial Z} - \frac{\partial W}{\partial X} \tag{3}$$

where W and U are local axial and radial velocity, respectively, and X and Z are the radial distance from the axisymmetric line and the

Table 1 Cases considered and their initial parameters

Exp	Nozzle geometry	Nozzle size a, mm	Initial velocity W_0, mm/s	Re
SNRe2358	Square nozzle	32	65.5	2358
SNRe3528	Square nozzle	32	98.0	3528
SNRe4716	Square nozzle	32	131.0	4716

streamwise distance from the nozzle exit, respectively. From the vorticity distributions, the total circulation can be obtained by integrating the vorticity contained within the lowest detectable contours for either positive or negative values. This contour level was determined to be at 2 s^{-1}. Sensitivity analysis had been made by selecting 1 s^{-1} as the boundary of the vortex ring, and the total circulation level was found to be insensitive to the choice of the cutoff level (the difference was within 5%). However, with 2 s^{-1}, separation between the vorticity contours of the head vortex from those of the trailing region could be clearly identified. In this analysis, the increment for the vorticity contours was also chosen to be 2 s^{-1} for all the three cases. The three invariants (i.e., the circulation Γ, energy E, and impulse I), which characterize the properties of the vortex ring, may be calculated from the experimental data as

$$\Gamma = \int_{\Omega} \omega \, dS \tag{4a}$$

$$E = \pi \int_{\Omega} (U^2 + W^2) X \, dS \tag{4b}$$

$$I = \pi \int_{\Omega} \omega X^2 \, dS \tag{4c}$$

where Ω is the integration area, where $|W| > 0$.

Following Gharib et al. [9], the dimensionless time t^* is defined by

$$t^* = t\bar{W}_0/D \tag{5a}$$

where t is the time from the jet initiation. The circulation and energy can also be normalized as

$$\Gamma_{\text{nd}} = \Gamma/(\bar{W}_0 D) \tag{5b}$$

and

$$E_{\text{nd}} = \frac{E}{I^{1/2}\Gamma^{3/2}} \tag{5c}$$

The total number of recordings was 600 for every case. The mean characteristics were averaged by more than 400 frames of the PIV images.

III. Results and Discussion

A. Case SNRe2358

Sequential images of the flow for this case are shown from Figs. 2a–2h. At $t^* = 1.16$ and Fig. 2a, the separation of boundary layers on either side of the nozzle wall caused the formation of vortices. Noticing that the region within the two vortices contained both jet and ambient fluids, this was indicated by the contrast in color within the vortex regions. The cross-sectional plane shows that axis switching had already taken place so that the leading square ring had turned 45 deg with respect to the jet exit plane. The secondary flow measured on the midplane of the leading vortex ring was essentially directing toward the jet axis (not shown here). At $t^* = 2.91$, it was noted that the traverse distance between the two head vortices grows farther apart, whereas that between the trailing vortices started to reduce; see Figs. 2a(i) and 2b(ii) for a better illustration and an indication of mutual interaction between the two vortex rings (Lim and Nickels [16]). From the cross-sectional view [Fig. 2b(ii)], the leading vortex ring looks as if it rotates by 45 deg as in Fig. 2a(ii) at instant $t^* = 1.16$. In fact, however, it is the third axis switching during the vortex ring evolution in terms of the images of some intermediate instants. Moreover, four pairs of streamwise vortices emerge along the direction normal to flat sides (A–A direction in Fig. 1b), as the result of the haul by the rapid spread of the vortex ring at flat sides.

By $t^* = 4.08$ and Fig. 2c(i), the difference in the traverse extent of the two vortex rings had become obvious. The cross-sectional view at plane B–B′ [Fig. 2c(ii)] shows that the trailing vortex ring had reverted back to its original square shape, as the second axis switching. Shedding of the excessive fluids in the form of the wake is also prominent, as indicated by the streamwise mushroom vortices appeared at the edge of the jet. And because of the shrinking effect of the vortices' interaction, the gap between vortex and jet stem is not distinct, but four pairs of streamwise vortices has appeared clearly at the corners of the jet stem (B–B direction in Fig. 1b). Compared with Fig. 2b(ii), it is reasonable that the streamwise vortices outside the trailing vortex ring can be regarded as the wake of the streamwise vortices induced by the leading vortex ring. The cross-sectional view at plane A–A′ [Fig. 2c(iii)] shows that the leading vortex ring has become more circular, reflecting its tendency to develop into an axisymmetric structure, and the streamwise vortices on the jet stem were seen to have strengthened further and become distorted.

During the leapfrogging process, the trailing vortex ring was entrained by the leading vortex ring, as shown in Fig. 2d(i) (at $t^* = 5.24$). It should be noted that at plane A–A′ [Fig. 2d(iv)], the trailing vortex ring occupying the center part cannot endure its ring configuration any more and it mixes up with the jet stem. Cross-sectional planes at B–B′ and C–C′ show that the streamwise vortices persisted at the four corners of the square jet stem. The existence of the streamwise vortices may not have affected the leapfrogging process. As it will be shown later, their existence would, however, be crucial for the pinch-off effect to occur. In contrast to Sau's results [8] on square sudden-expansion flow, in which the streamwise vortices dominate within a comparatively short distance and then dissipate very quickly, the two sets of streamwise vortices at corner portion (B–B direction) and flat-side portion (A–A direction), respectively, are capable of keeping their vortical structure throughout the starting stage of square jet flow.

As shown in Fig. 2e ($t^* = 6.19$) and Fig. 2f ($t^* = 7.64$), the third and the fourth pairs attempted to undergo the same process as the first and the second rings from $t^* = 9.09$ to $t^* = 9.82$ (Figs. 2g and 2h). The process was not successful such that they broke down together into turbulence. The fifth and the sixth rings also appeared to undergo the leapfrogging process but they had caught up with the turbulence region before the process could be completed. The breakdown to turbulence for the entire jet seemed to originate and propagate from the imperfect leapfrogging of the third and the fourth vortex rings.

Over the range of Reynolds numbers considered in this experimental study, the flow during the initial stage of the square jet flow appeared to be laminar, rather than turbulent. The focus of our work lay within a short time period after the jet was initiated (i.e., at the near field of the starting square jet). By comparing the characteristics of mixing transition (Konrad [17] and Dimotakis [18]) with the changing intensity of fluorescence from white and black in our results [Fig. 2d(iv)], it was found that the mixing of the jet fluids and ambient fluid reflected the entrainment and stirring process of the jet. As shown in the side-view images [such as Fig. 2c (i)], the color contrast in the spiral structure of the vortex ring core indicated the engulfment of irrotational fluids into the vortex ring

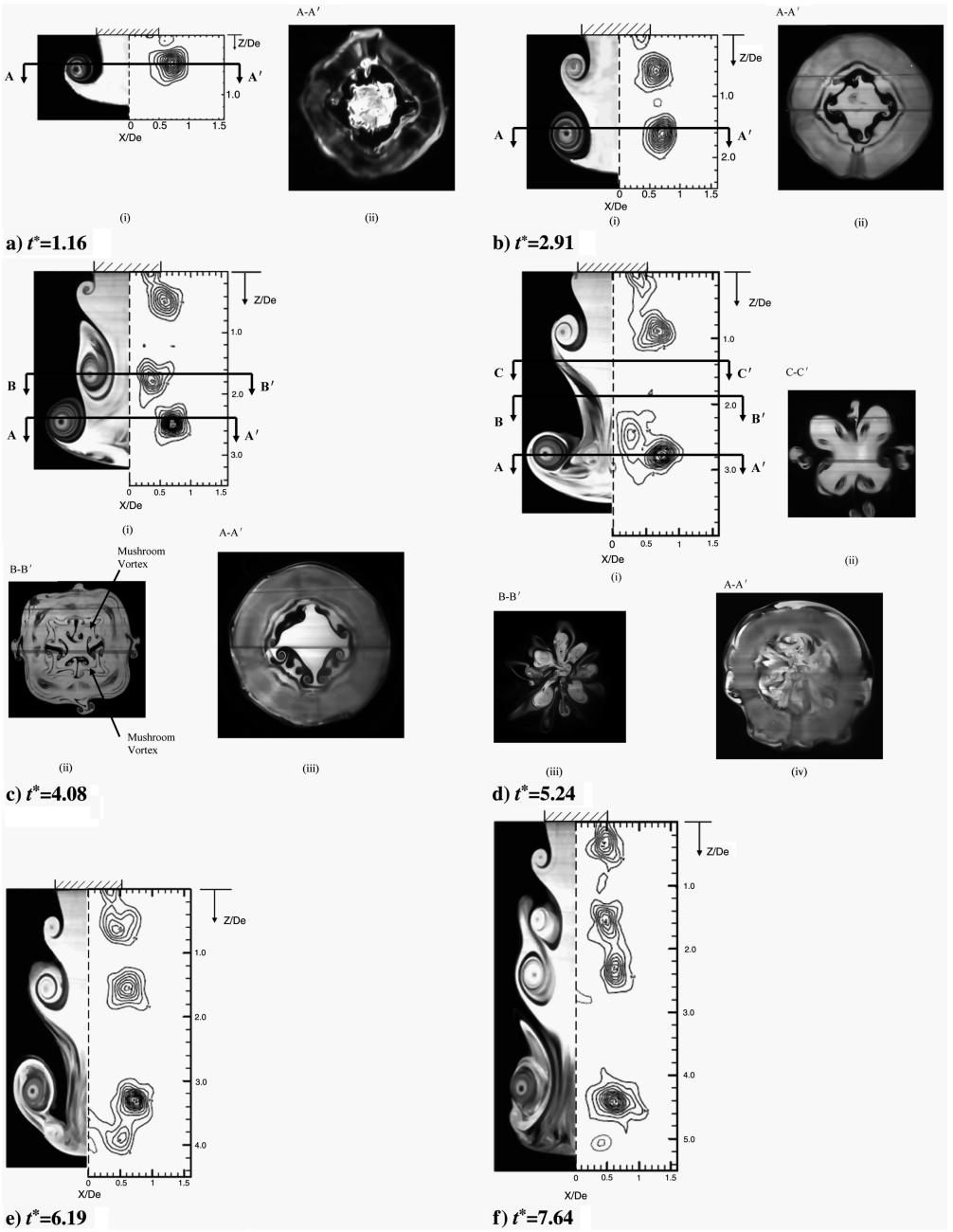
A-A′
Z/De
A
A′
1.0
0 0.5 1 1.5
X/De
(i)
(ii)
a) t*=1.16
b) t*=2.91
2.0
B
B′
3.0
C
C′
C-C′
B-B′
Mushroom Vortex
(iii)
(iv)
c) t*=4.08
d) t*=5.24
4.0
5.0
6.0
e) t*=6.19
f) t*=7.64
g) t*=9.09
h) t*=9.82

Fig. 2 $Re = 2358$.

core, and a large interfacial surface appeared between jet and ambient fluids. Through rapid diffusion of the fluorescent dye, the images showed a uniform gray in the vortex core region. It is believed that the smallest-scale mixing (i.e., molecular mixing), would mainly be responsible for the jet dynamics at the far field, in which the vortex rings have evolved into a fully developed turbulence state.

B. Case SNRe3528

The previous research [4] demonstrated that the axis-switching phenomenon is initiated by the deformation of large-scale coherent structures near the jet nozzle. Without the deformation and subsequent self-induction process, no axis switching is observed in noncircular jet flow, in which the vortex ring at both corner and side portion spread at a similar rate. For all cases conducted in the present experiment, the leading vortex ring and the first trailing vortex ring underwent continuous axis switching as they traveled downstream.

The sequential images of the flow for this case are shown in Figs. 3a–3d. At $t^* = 3.05$ [Fig. 3b(i)], the obvious difference that of the previous case was that it took a longer dimensionless time for the first trailing vortex ring to appear after the formation of the leading vortex ring. The distance between the leading vortices and the first trailing vortices were almost $2D_e$ compared with about $1.2D_e$ in the previous case. This can be attributed to the fact that higher vorticity was present at the boundary-layer regions at higher Reynolds numbers. The cross-sectional view [Fig. 3a(ii)] indicates the completion of the first axis switching, such as the situation in the case with $Re = 2358$. But it is noted that four pairs of streamwise vortices appears at the stem corners, as shown in Fig. 3a(ii) rather than at the flat-side portions as in case with $Re = 2358$. Under the affect of the first axis switching, these streamwise vortices serve to transport fluid from the jet stem to the leading vortex ring. As a consequence, between $t^* = 1.74$ and 5.22 [compare Figs. 3a(i), 3b(i), and 3c(i)], the thickness of the jet stem behind the leading vortex was found to shrink by almost 80%, based on the estimation from the flow visualization pictures. By $t^* = 8.71$ (see Fig. 3d), the jet stem behind the leading vortex had almost disappeared. At almost the same time, the first trailing vortices started to move closer toward the jet center axis. However, contrary to that observed in case SNRe2358, it is interesting to note that the trailing vortex ring did not accelerate forward but shed excessive fluids from the jet stem instead.

It is interesting to note that the first trailing vortices for case SNRe3528 did not surge forward rapidly as in the case SNRe2358. The distance between the leading vortices and first trailing vortices might be crucial for this phenomenon to occur. Another interesting observation was that the streamwise vortices appearing at the four corners of the jet stem did not appear only within the leading vortex ring region. As shown in the cross-sectional image on plane A–A′, at Figs. 3b(ii) and 3c(ii), it also appeared at a plane farther away from the leading vortex ring.

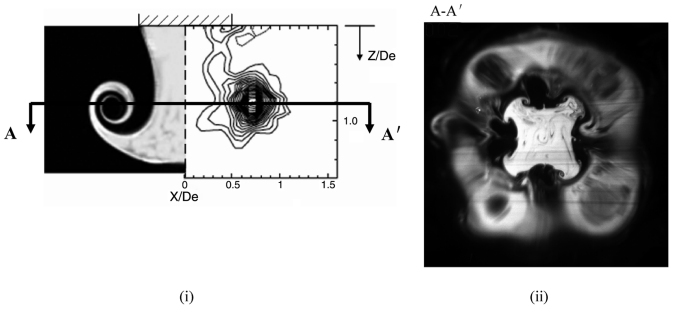

a) t^*=1.74

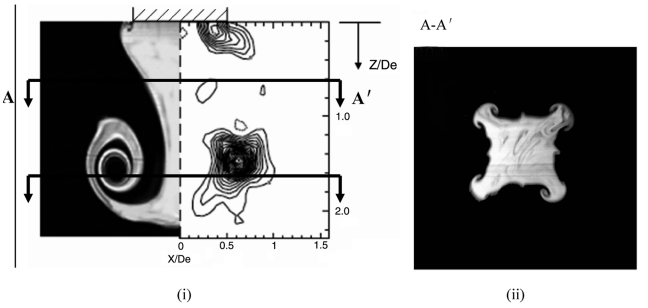

b) t^*=3.05

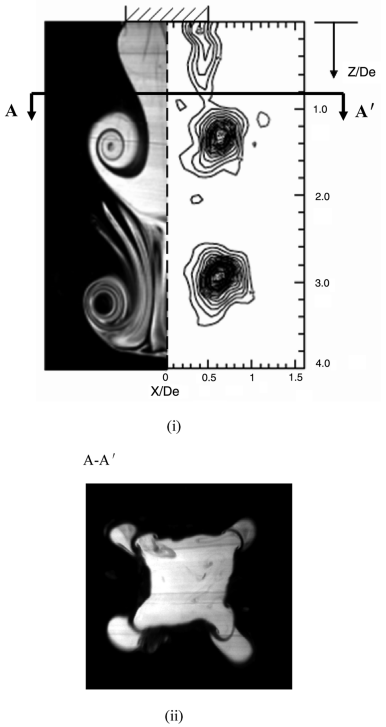

c) t^*=5.22

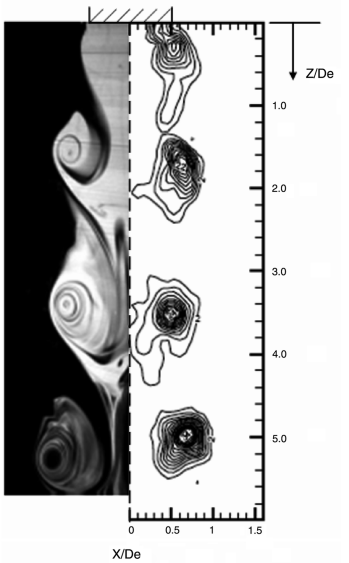

d) t^*=8.71

Fig. 3 $Re = 3528$.

C. Case SNR4716

At the highest Reynolds number case considered here, and as may have been expected, the time difference between the formation of the leading vortex ring and the first trailing vortices lengthened further [see from Fig. 4a(i) to Fig. 4b(i)]. Axis switching had taken place almost immediately after the jet was emerged so that the leading vortex ring had already turned 45 deg with respect to the nozzle exit plane [Fig. 4a(ii)]. Consequently, the jet stems were in close contact with the ring at the four corners. The self-induced deformation affected the evolution of the leading vortex ring such that by $t^* = 2.91$, the leading vortex ring had resumed the original square shape and had the orientation as the square nozzle exit plane [see Fig. 4b(ii)]. That was regarded as the second axis switching. The sequential cross-sectional images also reveal the counter-rotating vortex pairs at corners of the jet stem. By $t^* = 4.08$ and Fig. 4c(iv), the corner vortices continued to develop such that the jet stem was thinning rapidly. At the same time, the leading vortex ring was also moving faster forward under the influence of the self-induced velocities [compare Figs. 4a(i) and 4c(i)]. Like the streamwise vortices at the flat-side direction for case SNRe2358 [Fig. 2c(ii)], the effect of the corner vortices generated at the leading vortex region appeared to extend upstream [see the cross-sectional images at locations between the vortex rings in Figs. 4c(ii) and 4c(iii)]. At section C–C′ in Fig. 4c(ii), the four corners of the jet stem also came into close contact with the emerging vortex ring. The protrusions from the ring area in the directions of the four corners were the upstream effects from four corner vortex pairs at the jet stem. It should be pointed out that a new spanwise vortex was found to emerge at plane B–B′ in Fig. 4c(i). The spanwise vortex rolled up may have its origin to the occurrence of an inflexion point at the corresponding location, as the leading vortex ring is moving faster downstream because of self-induction.

Figure 4d provides the results for this case when the leading vortex was almost detached from the trailing jet. As shown in Fig. 4d(iv), the center region was almost empty of the jet fluids, indicating the vortex ring detached itself from the jet stem. At section B–B′ in Fig. 4d(iii), the four corner vortices were present, and there were fluids joining the four corners. It appeared to be the effect of the spanwise vortices rolled up and the entrainment of the excess fluids shed upstream. In the cross-sectional views on plane C–C′ [Fig. 4d(i)], there are clearly

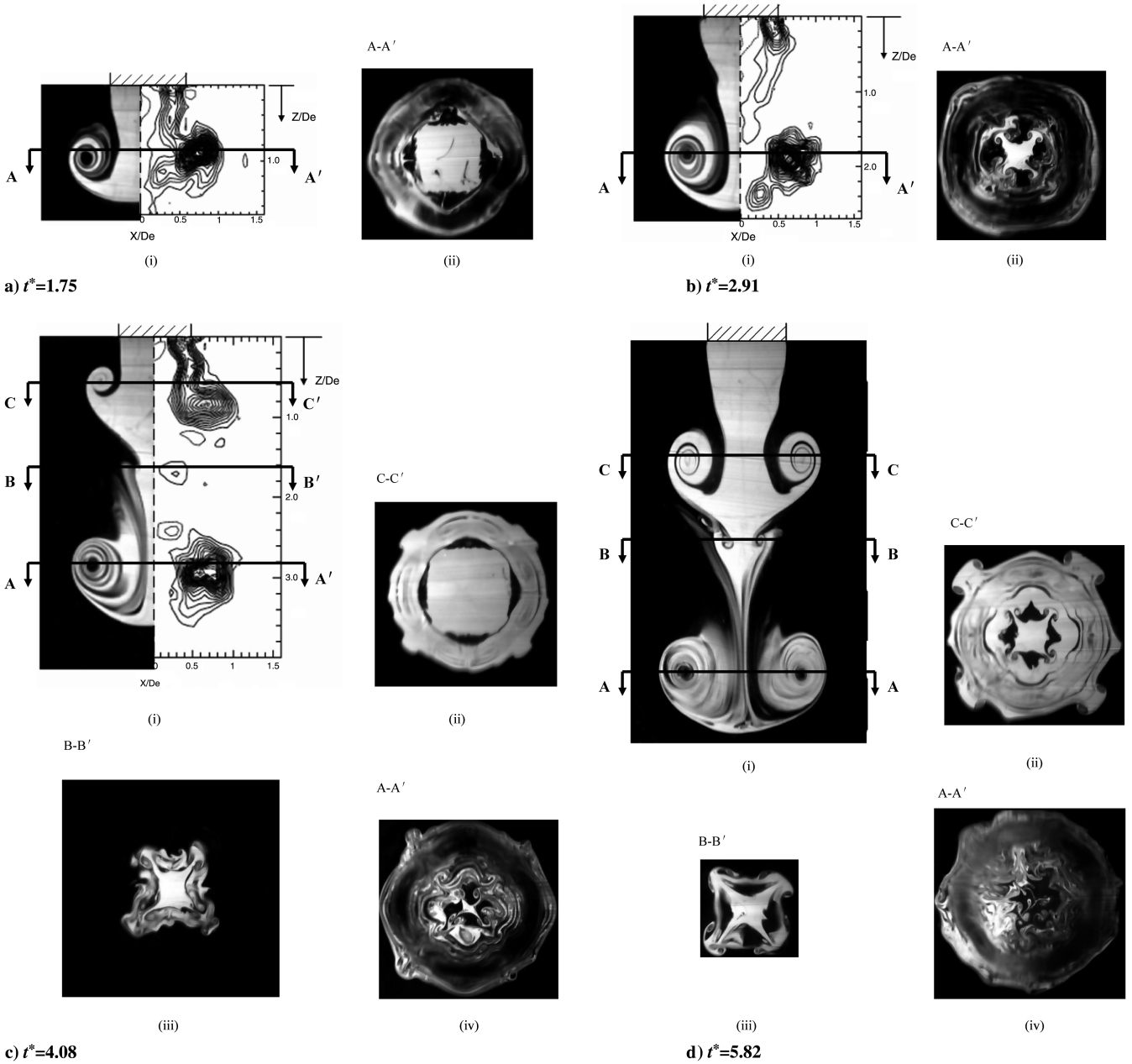

Fig. 4 ***Re*** **= 4716.**

three layers of fluids: the outer one consisted of the four corner vortices previously generated by the leading vortex ring and had shed downstream, the second layer consisted of the trailing vortex ring itself, whereas the inner one consisted of the newly generated corner vortices at the jet stem.

For the axisymmetric jet, Yu et al. [19] have investigated the effects of Reynolds numbers on the development of the vortex ring. Similar flow behaviors, such as the leapfrogging, have also been found in the present study. In addition, the results of present study also indicate the effects of Reynolds numbers on the appearance and development of streamwise vortices. At relatively lower Reynolds number cases, the initial jet stem was dominated by four pairs of outflow-type streamwise vortices and was along the direction normal to the flat sides (A–A direction), for which the influence could still be seen in the trailing jet at a later time [referring to vortices outside the trailing vortex ring in Fig. 2c(ii)]. For the other two cases at higher Reynolds numbers, the streamwise vortices first appeared at the corners of the jet stem (B–B direction), imposing long-term effects on the trailing jet flow also [Fig. 4d(ii)]. Quinn [2], Zaman [6], and Bradshaw [20] suggested that the skew-induced generation process at the four corners may be the possible source of the streamwise vortices. These vortices, generated from the distributed vorticity shed from the four corners of the nozzle by skewing of the shear layers, had a similar pattern to the streamwise vortices observed in the higher Reynolds numbers cases.

On the other hand, the streamwise vortices appearing on the centers of flat sides (A–A direction) could be explained by the interaction between the leading vortex ring and its adjacent jet stem. The simulation studies on the square sudden-expansion flow by Sau [8] showed that a group of passive forcing induced wall vortices, which had the pattern of outflowing type along the A–A direction, started immediately behind the expansion with a rapid growth rate. For the case at $Re = 2358$, the leading vortex ring might serve as the wall for the jet stem because of its relatively small translation velocity. The "wall vortices" were seen to quickly grow at the expense of the gradually decaying core streamwise vortices. For $Re = 3528$ and 4716, the influence of the leading vortex ring on the expanding jet stem became weaker and, as a consequence, was not able to induce the wall vortices.

D. Variation of Vortex Circulation and Energy

Figure 5a shows the variation of the total and leading vortex circulation against t^* for the three cases described earlier. The total circulation increased almost linearly with t^* as may have been expected for an impulsively started jet. The leading vortex had actually achieved its maximum strength at a relatively short time after the jet was initiated, for example at about $t^* = 1.6$ for SNRe2358 and at $t^* = 2.2$ for SNRe4716. The sudden increase at later time about $t^* = 4.6$ for the case SNRe2358 was because of the leapfrogging phenomenon in which the trailing vortex ring caught up with the first one providing additional strength to the leading vortex ring. For the other two cases, the strength of the head vortex rings was maintained at about the same level within the range of measurements. For cases SNRe3528 and SNRe4716, there was an initial over shoot before leveling off to a slightly lower value. The overshoot could be attributed to the effects of the radial pressure gradients when the jet was started impulsively. The jet discharge depended not only on the streamwise pressure gradients but also the pressure gradients in the radial direction. Krueger [21] had shown that the effects of the radial pressure gradients (or denoted as the over pressure effects) may account for 25% increase in the circulation generated. The present case showed a 20% rise.

The maximum circulation for the leading vortex ring appeared to be higher at higher Reynolds numbers. This is not unexpected as the boundary layers on the jet exit plane would be thinner at high Reynolds numbers and hence would give rise to stronger vorticity. It should be noted that the velocity profiles at the jet exit plane were essentially parabolic (Ai [14]). The CFD analysis by Zhao et al. [13] showed that parabolic profiles yielded a value of 1.95 for maximum circulation at Reynolds number about 3800 compared with about 1.8 at SNRe3528 in the present case. The similarity between these two values is interesting. Considering the fact that the generating mechanisms for the vortex rings were different (piston-driven vs gravity-driven), this may suggest a possible application of slug model for the present setup.

Normalized energy [cf. Eq. (5c)] for the three cases is also plotted in Fig. 5b. It can be seen from the figure that the energy level for respective cases is leveling at the same level at about $E_{\text{nd}} = 2.0$. This is not unexpected for jets having the same head. The energy level for the leading vortex was also plotted in the figure and is leveling to about the same level (i.e., after $t^* = 4.0$). It seemed that the energy for the leading vortex had reached an optimal value $t^* = 4.0$. It is interesting to note that the leapfrogging process for SNRe2358 did not cause a corresponding increase in the energy level. The increase for both circulation and energy may be balanced by the expansion in area so that the overall normalized energy of the vortex was maintained at the same level. Adopting the expression for the normalized kinetic energy, that is

$$\alpha = \frac{E_{\text{nd}}}{I^{1/2}\Gamma^{3/2}} \quad \text{and} \quad E_R = A\sqrt{\rho I \Gamma^3} \tag{6}$$

where A is a constant that can be determined from measurements, and α is the limiting value by which the formation process continuous as long as α exceeds A (α was estimated be equal at about 0.18 in the present investigation regardless of the Reynolds numbers). As shown earlier, even when A exceeds α, it did not necessarily lead to an

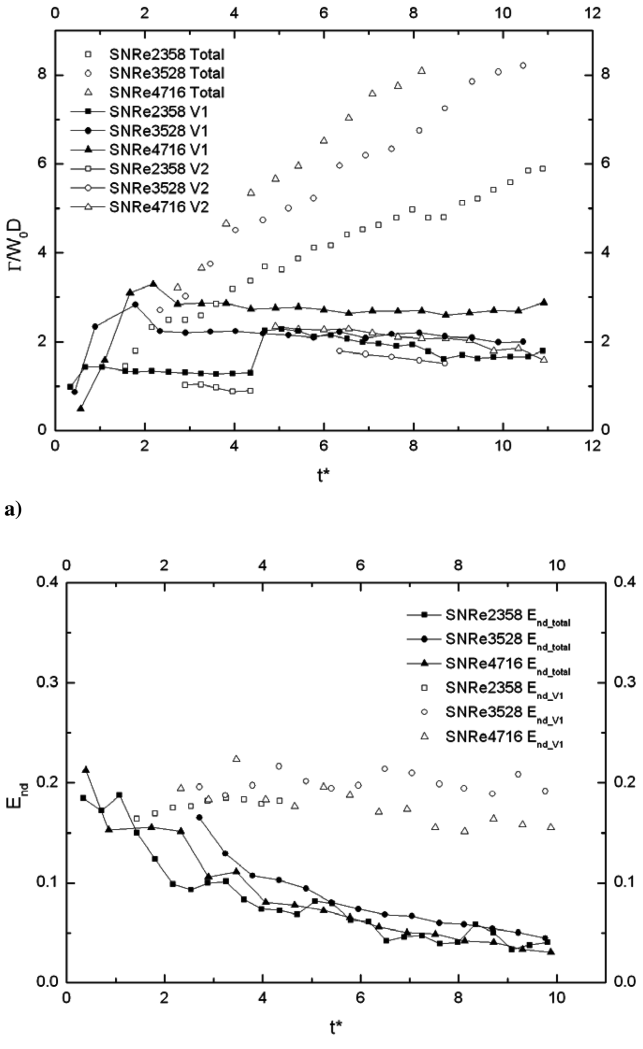

Fig. 5 Plots of a) temporal evolution of the circulation for total, V1, and V2, and b) variation of nondimensional energy with time.

immediate pinch-off for the leading vortex ring. This may be attributed to the presence of trailing jet instability which will be discussed in the following section.

E. Effects of K–H Vortices at the Trailing Jet

Figure 6a shows the variation of peak vorticity with time in the streamwise direction for case SNR4716. At earlier time and Fig. 6a (i), there was only one peak because of the presence of the leading vortex. The vorticity level increased very quickly because of the overpressure effects after the jet was initiated and had stabilized at certain value at a little smaller value after about $t^* = 4.0$. The second and the third peaks emerged at a later time [Fig. 6b(i)] as a consequence of the roll up of Kelvin–Helmholtz-type vortices, but they were about 30 and 40% lower in strength than that of the leading vortex, respectively, an obvious effect of the after pressure to the leading vortex. The distance between the leading vortex and the second vortex continued to increase, and the vorticity level between two vortex rings fell to nearly zero at $t^* = 6.04$, shown by Fig. 6c(i).

The presence of the trailing jet may have facilitated the onset of pinch-off for the leading vortex. Figure 6 also shows schematically the situations of having three rings simultaneously. In the presence of one leading vortex ring, after the vortex ring had achieved its maximum circulation strength and size, it continued to entrain fluids from the jet steam into the ring, but at the same time, excessive fluids were shed downstream as the wake of the vortex ring. The trailing jet stem started to thin down by two factors, the movement of the vortex ring downstream as well as entrainment and the subsequent shedding

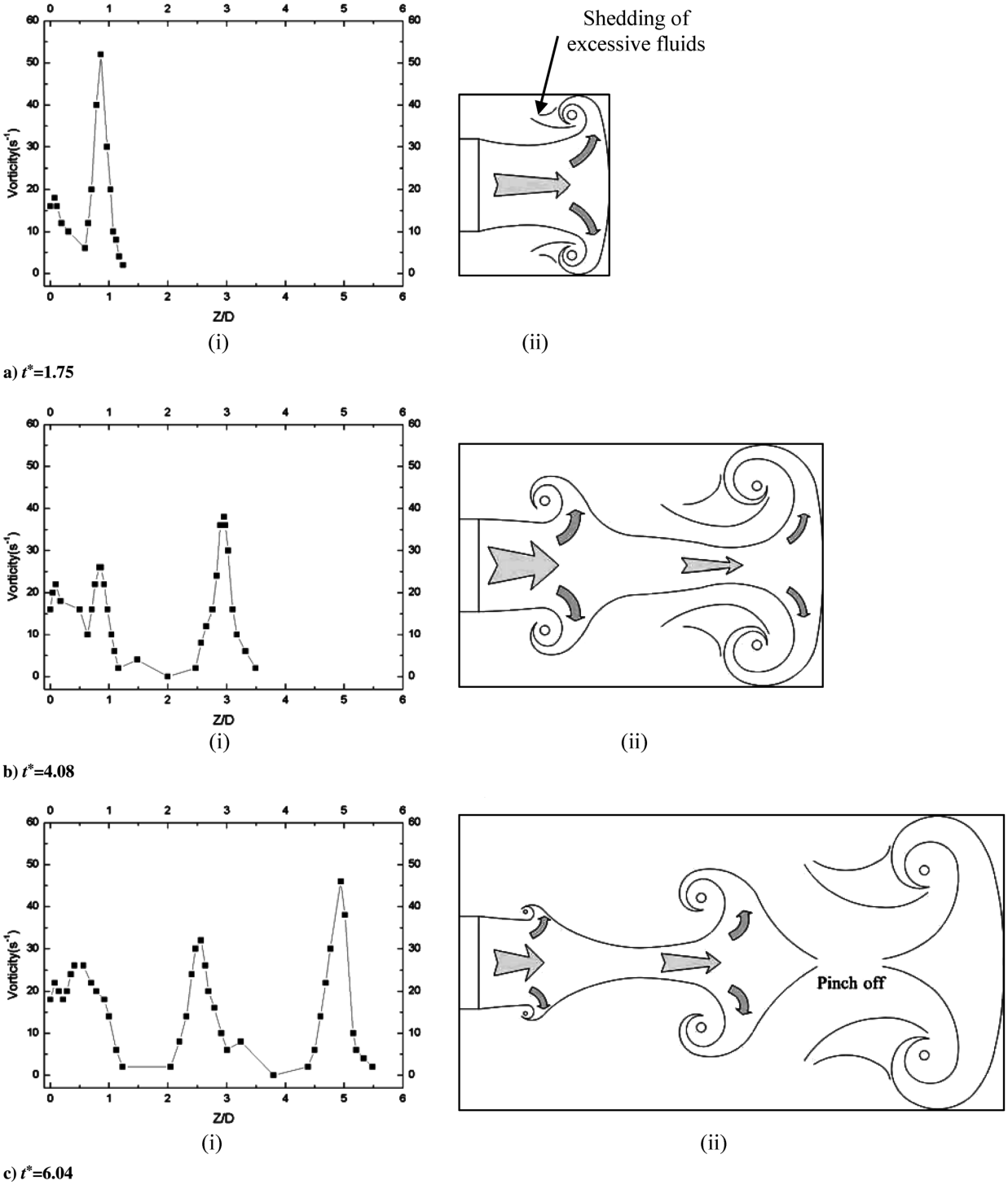

Fig. 6 Temporal evolution of the peak vorticity distribution in the streamwise location ($Re = 4716$).

of the fluids from the jet stem by the vortex ring, as depicted in Fig. 6b (ii). When the process involved additional trailing vortices, as shown in Fig. 6c(ii), the jet stem fluids between the first and second vortex rings were subjected to the additional entrainment by the second vortex ring, thereby thinning it even more quickly. It would therefore be expected that a starting jet without the trailing vortex would pinch off later than the case without the trailing vortex rings.

IV. Conclusions

Experiments have been conducted for a starting jet with a square cross section over a range of Reynolds numbers from 2000 to 5000. Axis switching was found to appear in all cases considered, and its existence was essential to the flow development of the starting jet. The leading vortex ring was axis switched almost immediately after the jet was initiated. The stronger and larger vortices generated at higher Reynolds numbers had entrained fluids from the jet stem causing the formation of contrarotating vortices at the four corners of the jet stem. It should be noted that these vortices were actually rotating in the opposite sense as those responsible for axis switching in a square jet.

As a result of the streamwise vortices, pinch-off for the leading vortex ring appeared faster than the circular jet under the same flow conditions. It should also be pointed out that the existence of Kelvin–Helmholtz vortices at the trailing jet may also be responsible for a faster pinch-off for the leading vortex. The same effect, however, was not found for Reynolds numbers below 3000. This may be attributed to the fact that the leading vortex ring was not strong enough to entrain fluids from the jet stem. The trailing vortex ring caught up soon for the leapfrogging effect to occur. It was also noticed that the transition to turbulence for Reynolds numbers below 3000 may have its origin from the imperfect leapfrogging between the third and fourth vortex rings so that they first broke down into turbulence and propagated upstream to the entire jet. The leading vortex, however, maintained its form for some distance downstream.

Acknowledgment

Financial support to this project from the Nanyang Technological University in the form of postgraduate scholarships for J. J. Ai and L. Gao is gratefully acknowledged.

References

[1] Quinn, W. R., and Militzer, J., "Experimental and Numerical Study of a Turbulent Free Square Jet," *Physics of Fluids*, Vol. 31, No. 5, 1988, pp. 1017–1025. doi:10.1063/1.867007

[2] Quinn, W. R., "Streamwise Evolution of a Square Jet Cross Section," *AIAA Journal*, Vol. 30, No. 12, 1992, pp. 2852–2857.

[3] Grinstein, F. F., Gutmark, E., and Parr, T., "Near-Field Dynamics of Subsonic, Free Square Jets: A Computational and Experimental Study," *Physics of Fluids*, Vol. 7, No. 6, 1995, pp. 1483–1497. doi:10.1063/1.868534

[4] Grinstein, F. F., and DeVore, C. R., "Dynamics of Coherent Structures and Transition to Turbulence in Free Square Jets," *Physics of Fluids*, Vol. 8, No. 5, 1996, pp. 1237–1251. doi:10.1063/1.868895

[5] Wang, X. K., Chua, L. P., and Yu, S. C. M., "On the Near Field of a Square Jet with Vortex Generating Tabs," *Fluid Dynamics Research*, Vol. 32, No. 3, 2003, pp. 99–117. doi:10.1016/S0169-5983(03)00015-7

[6] Zaman, K. B. M. Q., "Axis Switching and Spreading of an Asymmetric Jet: the Role of Coherent Structure Dynamics," *Journal of Fluid Mechanics*, Vol. 316, June 1996, pp. 1–27. doi:10.1017/S0022112096000420

[7] Gutmark, E. J., and Grinstein, F. F., "Flow Control with Noncircular Jets," *Annual Review of Fluid Mechanics*, Vol. 31, 1999, pp. 239–272. doi:10.1146/annurev.fluid.31.1.239

[8] Sau, A., "Generation of Streamwise Vortices in Square Sudden-Expansion Flows," Pt. 2, *Physical Review E (Statistical Physics, Plasmas, Fluids, and Related Interdisciplinary Topics)*, Vol. 69, No. 5, 2004, Paper 056307.

[9] Gharib, M., Rambod, E., and Shariff, K., "A Universal Time Scale for Vortex Ring Formation," *Journal of Fluid Mechanics*, Vol. 360, Apr. 1998, pp. 121–140. doi:10.1017/S0022112097008410

[10] Mosheni, K., and Gharib, M., "A Model for Universal Time Scale of Vortex Ring Formation," *Physics of Fluids*, Vol. 10, No. 10, 1998, pp. 2436–2438. doi:10.1063/1.869785

[11] Ai, J. J., Yu, S. C. M., and Law, A. W.-K., "Vortex Dynamics in Starting Square Water Jets," *Physics of Fluids*, Vol. 17, No. 1, Jan. 2005, Paper 014106.

[12] Linden, P. F., and Turner, J. S., "The Formation of "Optimal" Vortex Rings, and the Efficiency of Propulsion Devices," *Journal of Fluid Mechanics*, Vol. 427, Jan. 2001, pp. 61–72. doi:10.1017/S0022112000002263

[13] Zhao, W., Frankel, S. H., and Mongeau, L. G., "Effects of Trailing Jet Instability on Vortex Ring Formation," *Physics of Fluids*, Vol. 12, No. 3, 2000, pp. 589–596. doi:10.1063/1.870264

[14] Ai, J. J., "On Starting Square Jets and Forced Plumes," Ph.D. Dissertation, School of Mechanical and Aerospace Engineering, Nanyang Technological Univ., Singapore, 2006.

[15] Karasso, P. S., and Mungal, M. G., "PLIF Measurements in Aqueous Flows Using the Nd:YAG Laser," *Experiments in Fluids*, Vol. 23, No. 5, 1997, pp. 382–387. doi:10.1007/s003480050125

[16] Lim, T. T., and Nickels, T. B., "Vortex Rings," *Fluid Vortices*, edited by S. I. Green, Kluwer, Dordrecht, The Netherlands, 1995.

[17] Konrad, J. H., "An Experimental Investigation of Mixing in Two-Dimensional Turbulent Shear Flows with Applications to Diffusion-Limited Chemical Reactions," Ph.D. Dissertation, California Inst. of Technology, Pasadena, CA, 1976.

[18] Dimotakis, P. E., "The Mixing Transition in Turbulent Flows," *Journal of Fluid Mechanics*, Vol. 409, Apr. 2000, pp. 69–98. doi:10.1017/S0022112099007946

[19] Yu, S. C. M., Law, A. W.-K., and Ai, J. J., "Vortex Formation Process in Gravity-Driven Starting Jets," *Experiments in Fluids*, Vol. 42, No. 5, 2007, pp. 783–797. doi:10.1007/s00348-007-0290-6

[20] Bradshaw, P., "Turbulent Secondary Flows," *Annual Review of Fluid Mechanics*, Vol. 19, 1987, pp. 53–74. doi:10.1146/annurev.fl.19.010187.000413

[21] Krueger, P. S., "An Over-Pressure Correction to the Slug Model for Vortex Ring Circulation," *Journal of Fluid Mechanics*, Vol. 545, Dec. 2005, pp. 427–443. doi:10.1017/S0022112005006853

R. Lucht
Associate Editor